

SI Appendix

Oscillations make a self-scaled model for honeybees' visual odometer reliable regardless of flight trajectory

Lucia Bergantin, Nesrine Harbaoui, Thibaut Raharijaona and Franck Ruffier

S1. Honeybees' self-oscillation

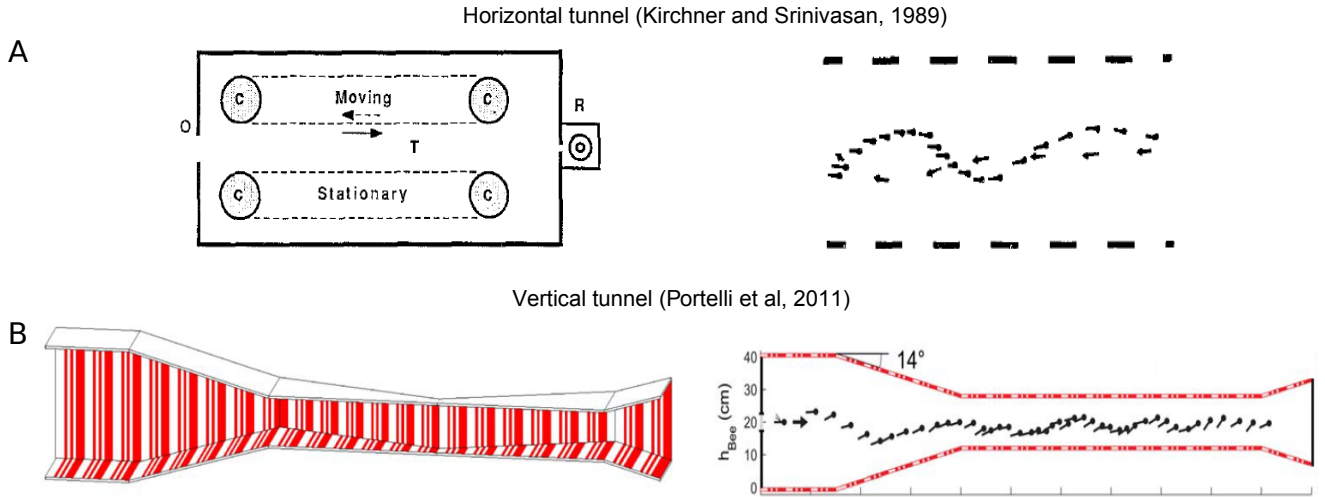


Figure S1: A.i) Honeybees were trained to enter a horizontal tunnel via the opening O and fly along it to the box R containing a sugar water reward. A.ii) The oscillatory trajectory of one honeybee flying along the horizontal tunnel (adapted from [1]). B.i) Perspective view of the whole doubly-tapered tunnel in which the experiments were carried out. B.ii) Side view of a honeybee's oscillatory trajectory (adapted from [2]).

S2. Extended Kalman Filter equations

The following processing steps were performed by the Extended Kalman Filter (EKF) to estimate the simulated bees' height of flight h , based on the downward-perceived optic flow divergence as the measurements and the stroke amplitude as the inputs feeding the vertical dynamics. In order to apply the EKF, the system was discretised and linearised around an estimated nominal trajectory in order to obtain a linear model for the error. One EKF equation was slightly adapted by adding an absolute function to the first state (the ground height) in the previous state estimate, in order to account for the fact that the ground height can only be positive (see expression of X_{k-1} in eq. Eq. S1). In practice, this helps to obtain a much faster and more reliable convergence of the EKF estimates. The covariance of the measurement noise R was $3 \cdot 10^{-6}$, and that of the process noise Q was $1 \cdot 10^{-3}$.

Prediction step

(a) One-step-ahead predictions

$$X_{k|k-1} = f(X_{k-1}, u_{k-1}) \quad (\text{Eq. S1})$$

with $X_{k-1} = \begin{bmatrix} |h| \\ v_h \end{bmatrix}$ (because the height is always positive)

(b) Covariance matrix of the state prediction error vector

$$P_{k|k-1} = F_{k-1} P_{k-1|k-1} F_{k-1}^T + Q_{k-1} \quad (\text{Eq. S2})$$

where F_k is the Jacobian matrix of $f(\cdot)$

$$F_{k-1} = \frac{\partial f}{\partial X} \Big|_{X=X_{k-1|k-1}} \quad (\text{Eq. S3})$$

Correction step

(c) Measurement update

$$X_{k|k} = X_{k|k-1} + W_k(Z_k - g(X_{k|k-1})) \quad (\text{Eq. S4})$$

(d) Covariance matrix of the state estimation error vector

$$P_{k|k} = P_{k|k-1} + W_k[H_k P_{k|k-1} H_k^T + R_k]W_k^T \quad (\text{Eq. S5})$$

$$W_k = P_{k|k-1} H_k^T [H_k P_{k|k-1} H_k^T + R_k]^{-1} \quad (\text{Eq. S6})$$

where H_k is the Jacobian matrix of the nonlinear function defined as follows:

$$H_k = \frac{\partial g}{\partial X} \Big|_{X=X_{k|k-1}} \quad (\text{Eq. S7})$$

where:

W_k is the Kalman gain.

$Z_k - g(X_{k|k-1})$ is called the innovation of EKF.

$H_k P_{k|k-1} H_k^T + R_k$ is the covariance of the innovation.

S3. Robustness of the *SOFIa* visual odometer at the various self-oscillation frequencies applied

To further determine its robustness at various self-oscillation frequencies, the *SOFIa* visual odometer was tested in simulation under the 630 parametric conditions with the following four sets of self-oscillation parameters: $f_{osc} = 1Hz$ and $A_{osc} = 18 \text{ deg}$; $f_{osc} = 2Hz$ and $A_{osc} = 40 \text{ deg}$; $f_{osc} = 3Hz$ and $A_{osc} = 60 \text{ deg}$; $f_{osc} = 4Hz$ and $A_{osc} = 80 \text{ deg}$. Figure S2 shows the distributions of the *SOFIa* model outputs with the four self-oscillation frequencies studied. Their spreads were not found to differ significantly from each other, and therefore they did not depend on the self-oscillation frequency (Brown-Forsythe-test, $df = \{3, 2516\}$, $p\text{-value} = 0.899$).

Figure S3 shows examples of simulations performed over a $100m$ -long ground surface including 3 small hills with gentle slopes separated by flat areas under no wind, tail wind and head wind conditions at 4 different self-oscillation frequencies, f_{osc} : $1Hz$, $2Hz$, $3Hz$ and $4Hz$. The simulations were performed with a peak height h_{peak} of $1m$, a wind speed gain k_{wind} of $-1m/s$, $0m/s$ and $1m/s$, a translational optic flow setpoint ω_T^{set} of 2.5 radians/sec and a pitch u_Θ of 30 deg . Figure S3 shows that in each of the four self-oscillation frequencies under consideration, the error with respect to the goal located at a distance of $100m$ ranged between 0.1% and 2.2% .

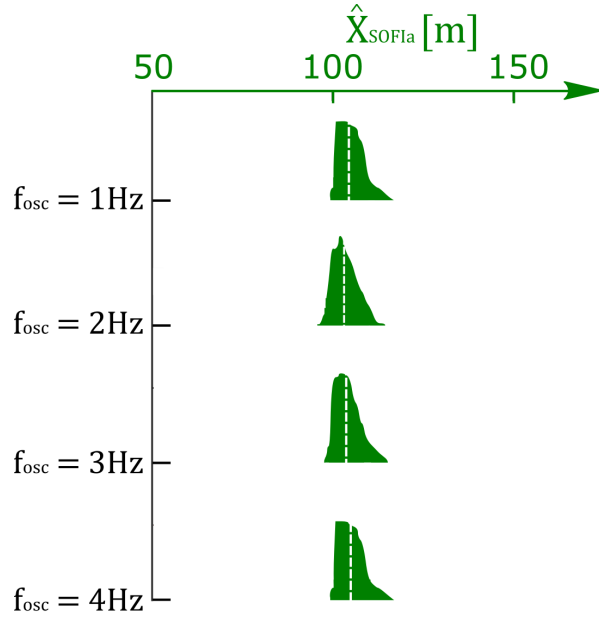


Figure S2: The plots show the statistical dispersions of the outputs of the *SOFia* model tested in simulation under the 630 parametric conditions with f_{osc} of 1Hz, 2Hz, 3Hz and 4Hz. The median values of the distributions ranged between 102.79m and 104.8m, while their MAD ranged between 3.03m and 3.09m. The spreads of the four distributions did not depend on the self-oscillation frequency because they were not found to differ significantly from each other (Brown-Forsythe-test, $df = \{3, 2516\}$, $p\text{-value} = 0.899$).

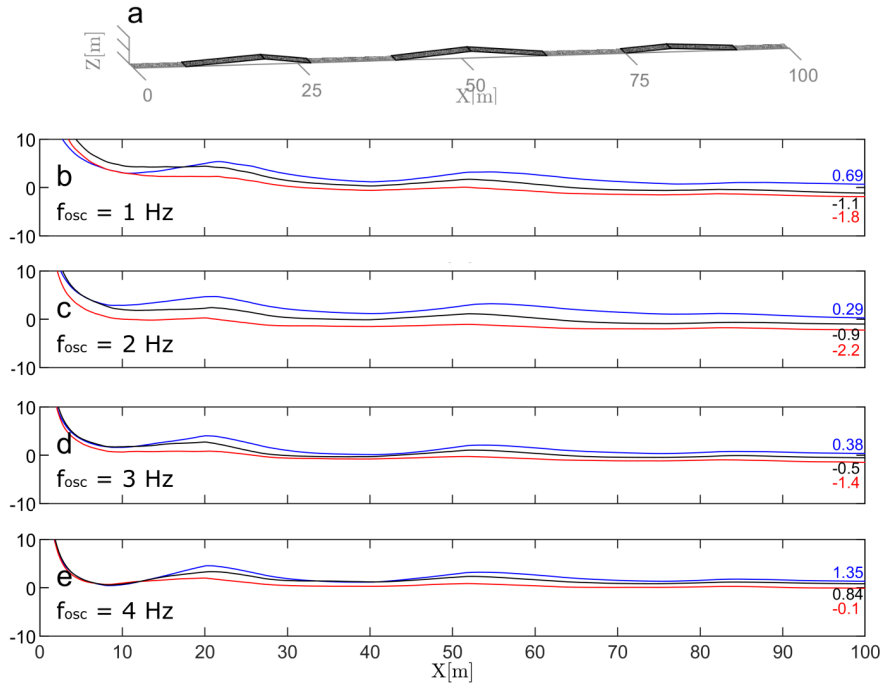


Figure S3: (a) Examples of simulated oscillatory flights over a 100m-long ground surface including 3 small hills with gentle slopes separated by flat areas under no wind (in black), tail wind (in blue) and head wind (in red) conditions were plotted. The self-oscillatory movements were simulated by a sine wave with (b) $f_{osc} = 1Hz$ and $A_{osc} = 18$ deg, (c) $f_{osc} = 2Hz$ and $A_{osc} = 40$ deg, (d) $f_{osc} = 3Hz$ and $A_{osc} = 60$ deg and (e) $f_{osc} = 4Hz$ and $A_{osc} = 80$ deg. At each oscillation frequency under consideration, the error in the estimated flight distances with respect to the ground truth was normalised and expressed in %. The error ranged between 0.1% and 2.2%.

S4. Final % errors in the flight distances estimated under three different wind conditions

	head wind	no wind	tail wind
$\hat{X}_{SOFIa} (f_{osc} = 1Hz)$ (% error \pm % rMAD)	-1.8 ± 2.69	-1.1 ± 2.75	0.69 ± 3.16
$k_{comparisons} \cdot OFacc (f_{osc} = 1Hz)$ (% error \pm % rMAD)	20.6 ± 28.7	-3.3 ± 22.45	-26 ± 19.72
Open field, data from [3] (% error \pm % rSD)			3 ± 25.7 ¹
Narrow tunnel, data from [4] (% error)	6.66 ²	-3.33 ³	-14.4 ⁴

Table S1: Table of the final % errors in the flight distances assessed by the *SOFIa* model, the *OFacc* model calibrated with $k_{comparisons}$, based on data published by [3] and [4]. To obtain the datasets with the *SOFIa* and the *OFacc* models, honeybee flights were simulated over a 100m-long ground surface including 3 small hills with gentle slopes separated by flat areas under no wind, tail wind and head wind conditions. With both models, the relative Median Absolute Deviation (rMAD) was computed under the three wind conditions under consideration. In [3] data were collected in the open field under cross-tail wind conditions. The final % error was retrieved, and the relative Standard Deviation (rSD) was computed. In [4], the data were collected in a narrow tunnel 3.2m long, 22cm wide and 20cm high. The final % error was determined under no wind, tail wind and head wind conditions. It was difficult to make fair comparisons between the four datasets in question because the conditions under which the experiments in the studies by [3] and [4] were conducted and the methods used to analyse the data were very different.

¹Data from [3] collected under a mean crosswind of 3.3m/s oriented at 38 deg with respect to the normal from the hive to the feeder, i.e. with a mean tail wind component of 2.6m/s.

²Data recomputed from Figure 3a in [4] collected under a head wind of 0.7m/s.

³Data recomputed from Figure 3a in [4] collected in still air.

⁴Data recomputed from Figure 3a in [4] collected under a tail wind of 0.65m/s.

S5. Simulations under tail and head wind conditions with respect to time

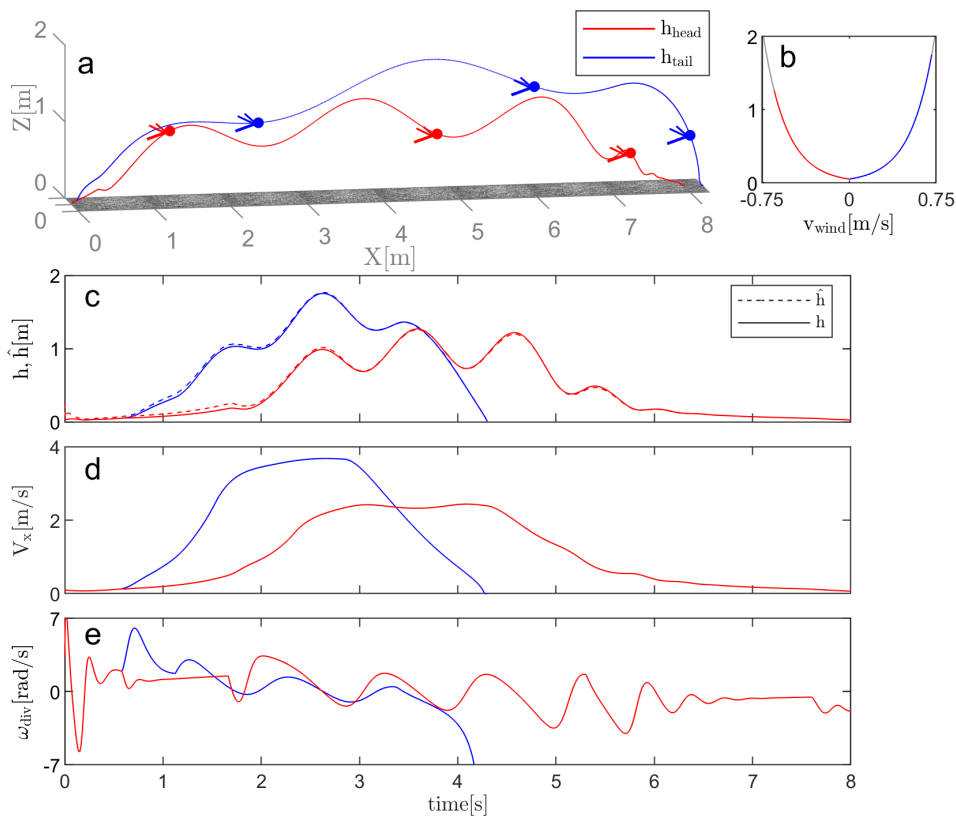


Figure S4: Oscillating forward flights of honeybees were simulated over a 8m-long flat ground (see Simulated honeybee flight parameters section in *Material and Methods*). a) The trajectory including take-off, cruise flight and landing was simulated under tail (blue) and head (red) wind conditions. The results of the simulations were plotted here with respect to the distance flown. b) The wind was modelled as in equation 4.7. c) The results of the simulations were plotted here with respect to time. To reach the goal position at 8m, the simulated honeybee took about 4s under tail wind and about 7.5s under head wind conditions. d) The ground speed, V_x , obtained during cruise flight depended on the wind conditions. The ground speed was higher in the case of tail wind (blue), which made the simulated honeybee fly at a higher altitude due to the optic flow regulation process; the ground speed was lower in the case of head wind (red), which made the honeybee fly at a lower altitude. e) The optic flow divergence patterns observed were due to the vertical self-oscillatory movements. At a given optic flow setpoint, the amplitude of the optic flow divergence was greater in the case of head wind due to the honeybee being closer to the ground.

S6. Statistical dispersion: comparisons in terms of u_{Θ} and h_{peak}

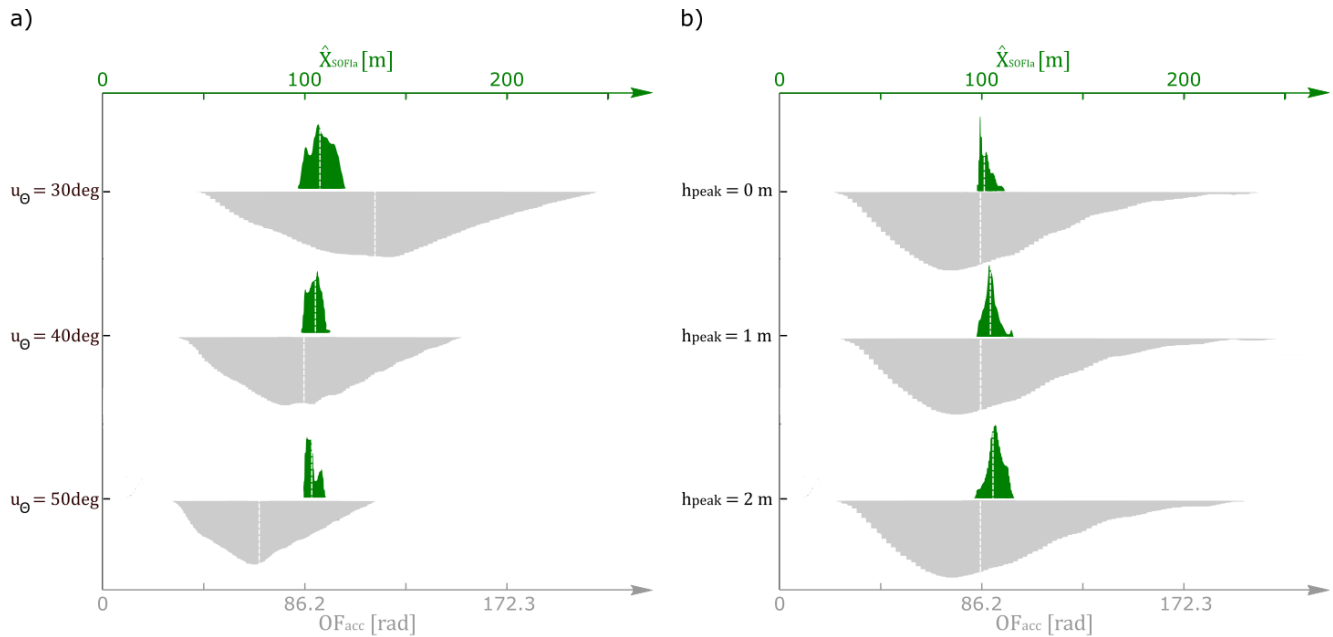


Figure S5: The plots give the statistical distributions of the results obtained with the *SOFia* model (in green) and the *OFacc* model (in grey) with various values of u_{Θ} and h_{peak} . Both models were tested in simulation under a total number of 630 parametric conditions, as described in Section 3.c. The *OFacc* model was calibrated with $k_{comparisons}$ (see *Materials and Methods*) so as to be able to make direct comparisons with the *SOFia* model. (a) The median values of the statistical dispersions of the data obtained with the *SOFia* model with various values of the pitch u_{Θ} (which drives the forward speed) ranged between $103.6m$ and $107.78m$, while those of the *OFacc* model ranged between $77.6m$ and $134.7m$. The MAD of the *SOFia* model ranged between $2.22m$ and $4.07m$, whereas the MAD of the *OFacc* model ranged between $17.83m$ and $34.5m$. At a given optic flow setpoint, in the case of low body pitch, the slower the honeybee flies, the longer the *OFacc* model accumulates the optic flow magnitude and hence, the more greatly the flight distance is overestimated. Conversely, in the case of high body pitch, the faster the honeybee flies, the quicker the honeybee reaches the food source, and the shorter the time during which the *OFacc* model integrates the magnitude of the optic flow mathematically and hence, the more greatly the flight distance is underestimated. Therefore, in the case of both low and high speeds, the output of the *OFacc* model deviates increasingly with time from the actual distance flown by the simulated honeybee. Overall, the pitch parameter significantly affected the median values of the *OFacc* model distributions (Friedman-test, $df=2$, $p\text{-value} \ll 0.001$), whereas the output of the *SOFia* model varied very little depending on this parameter. Under each of the u_{Θ} conditions considered, the median values of the two models' outputs differed significantly (Wilcoxon test, $p\text{-value} \ll 0.001$, $Z=13.76$ in the case of each pitch). (b) The median values of the statistical distributions of the data obtained with the *SOFia* model with various values of h_{peak} ranged between $101.6m$ and $106.75m$, while those of the data obtained with the *OFacc* model ranged between $99.58m$ and $99.76m$. The MAD of the *SOFia* model was consistently lower than $3.26m$, whereas the MAD of the *OFacc* model ranged between $29.99m$ and $31.01m$. Under each of the h_{peak} conditions tested in simulation, the spread of the two models' outputs differed significantly (Brown-Forsythe-test, $df:278$, $p\text{-value} \ll 0.001$, $F=182.37;181.80;170.71$, with $h_{peak} = 0m; 1m; 2m$, respectively).

References

- [1] Kirchner, W. & Srinivasan, M. 1989 Freely flying honeybees use image motion to estimate object distance. *Naturwissenschaften*, **76**(6), 281–282.
- [2] Portelli, G., Ruffier, F., Roubieu, F. L. & Franceschini, N. 2011 Honeybees' speed depends on dorsal as well as lateral, ventral and frontal optic flows. *PloS one*, **6**(5), e19 486.
- [3] Riley, J. R., Greggers, U., Smith, A. D., Reynolds, D. R. & Menzel, R. 2005 The flight paths of honeybees recruited by the waggle dance. *Nature*, **435**(7039), 205–207.
- [4] Srinivasan, M., Zhang, S. & Bidwell, N. 1997 Visually mediated odometry in honeybees. *Journal of Experimental Biology*, **200**(19), 2513–2522.